GA–A27666

efit.py KINETIC EFIT METHOD

by
T.H. OSBORNE

Work supported by
the General Atomics Internal Funding

SEPTEMBER 2013

GENERAL ATOMICS

GA–A27666

efit.py KINETIC EFIT METHOD

by
T.H. OSBORNE

Work supported by
the General Atomics Internal Funding

GENERAL ATOMICS PROJECT 40010
SEPTEMBER 2013

GENERAL ATOMICS

The primary goal of the kinetic EFIT [8] method in the efit_kinetic.py module is to efficiently generate MHD equilibrium for use in stability studies of the H-mode pedestal region. Pedestal stability is sensitive to the current density profile in this region. While MSE coupled with external magnetic measurements provide sufficient spatial resolution to determine the current density profile in the plasma core, the short spatial scales and large radial electric field in the pedestal region have so far prevented accurate determination of the pedestal current density profile from this data alone. It is hoped that in the future, measurements of the pedestal current density profile with the Lithium beam system[1] will become routine, however an alternative approach is needed at present. In the approach implemented in the efit_kinetic.py module, the core current density profile is determined by MSE plus external magnetics, while the current density profile in the pedestal is calculated using models for Ohmic, bootstrap, and beam/RF driven currents.

MKS units are used in this memo with temperature in keV, density in $10^{20}/m^3$, and pressure in kPa.

Outline:

1. **Currents and Magnetic Fields**: Forms for $\vec{j}$ and $\vec{j} \cdot \vec{B}$ are derived.
2. **Kinetic MHD Equilibrium Solution**: Outlines the approach for producing an MHD equilibrium using the experimentally measured pressure profile plus an H-mode pedestal current density constrained using models for the bootstrap current. Discusses the connection between flux surface average parallel and toroidal current density.
3. **Computing j_{PAR}**: Shows how the parallel current density is computed from the bootstrap, Ohmic and driven current densities.
4. **Expressions for j_{BS}**: Gives complete expressions for bootstrap current from the Sauter[3] and Koh[4] models.
5. **Expressions for conductivity σ_0 :** Gives complete expressions for the neoclassical conductivity.
6. **Important quantities for edge stability:** Gives expressions for several quantities which are important for stability of the H-mode pedestal.
7. **efit_jsauter.py inputs and outputs:** Inputs and outputs for the python module used to compute the pedestal current density.
8. **ONETWO code related parameters:** Shows how the current densities output by the ONETWO transport code are related to those described in this memo.
9. **Running efit.py to produce a kinetic EFIT:** Outlines how to run the python script efit.py to put it all together to produce a kinetic MHD equilibrium using EFIT.

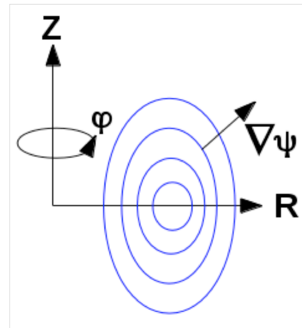

1. Currents and Magnetic Fields

The geometry is shown at right. The **Z** axis is assumed to be vertically upward with φ wrapping around it in the right hand sense, and **R** is the major radius. Consistent with the convention used in the EFIT code, the MHD poloidal flux, ψ, increases moving outwards from the magnetic axis regardless of the sign of the plasma current.

The total magnetic field is given by

$$\vec{B} = \overrightarrow{B_P} + \overrightarrow{B_\varphi} = s\nabla\varphi \times \nabla\psi + f\nabla\varphi \tag{1.1}$$

$$B_R = s\frac{1}{R}\frac{\partial\psi}{\partial Z} \tag{1.2}$$

$$B_Z = -s\frac{1}{R}\frac{\partial\psi}{\partial Z} \tag{1.3}$$

$$B_\varphi = \frac{f(\psi)}{R} \tag{1.4}$$

where $s = sign(I_P)$. Here positive I_P and B_φ are in the $\hat{\varphi}$ direction. The normal current and toroidal field direction on DIII-D has s>0 and f<0.

From Ampère's law, $\nabla \times \vec{B} = \mu_0\vec{j}$,

$$\vec{j} = j_\varphi R\nabla\varphi - s\frac{f'}{\mu_0}\overrightarrow{B_p} = \frac{s}{\mu_0}\left(\Delta^*\psi\nabla\varphi - f'\overrightarrow{B_p}\right) \tag{1.5}$$

where $' \equiv d/d\psi$ and

$$s\mu_0 R j_\varphi = \Delta^*\psi = R\frac{\partial}{\partial R}\left(\frac{1}{R}\frac{\partial\psi}{\partial R}\right) + \frac{\partial^2\psi}{\partial Z^2} \tag{1.6}$$

Using the equations for $\vec{B}$ and $\vec{j}$ above we have

$$\vec{j}\cdot\vec{B} = \frac{j_\varphi f}{R} - s\frac{f'}{\mu_0}{B_p}^2 = f\left(\frac{j_\varphi}{R} - s\frac{ff'}{\mu_0 R^2}\frac{{B_p}^2}{{B_\varphi}^2}\right) \tag{1.7}$$

and

$$\vec{j}\times\vec{B} = p'\nabla\psi = -\left(\frac{sj_\varphi}{R} + \frac{ff'}{\mu_0 R^2}\right)\nabla\psi \tag{1.8}$$

$$-p' = s\frac{j_\varphi}{R} + \frac{ff'}{\mu_0 R^2} \tag{1.9}$$

Except at very high β_{POL}, the toroidal and poloidal current contributions to the pressure balance represented by the two terms on the right hand side of equation (1.9) are of the same order, with more typically the toroidal current term dominating. With this in mind we see that the poloidal current contribution to $\vec{j}\cdot\vec{B}$ represented by the second term on the right hand side of equation (1.7) is small compared to the toroidal current contribution by at least the order of $\frac{{B_p}^2}{{B_\varphi}^2}$. This fact is important in the iteration scheme described later where $\vec{j}\cdot\vec{B}$ is computed with the poloidal current evaluated using an equilibrium from a previous iteration.

Substituting the toroidal current from equation (1.9) into equation (1.7) gives an expression for the current parallel to B consistent with force balance

$$\vec{j}\cdot\vec{B} = -sfp' - s\frac{f'}{\mu_0}B^2 \tag{1.10}$$

Taking the flux surface average defined by

$$\langle A\rangle = \frac{\oint \frac{Adl}{|B_p|}}{\oint \frac{dl}{|B_p|}} = \frac{1}{V_P}\oint \frac{Adl}{|B_p|};\ V_P = \frac{1}{2\pi}\frac{\partial V}{\partial \psi} \tag{1.11}$$

of equation (1.10) gives

$$-s\frac{f'}{\mu_0} = \frac{sfp' + \langle \vec{j}\cdot\vec{B}\rangle}{\langle B^2\rangle} = \frac{\vec{j}\cdot\overrightarrow{B_p}}{{B_p}^2} \tag{1.12}$$

where the last equality comes from equation (1.5). Substituting equation (1.12) back into equation (1.10) gives

$$\vec{j}\cdot\vec{B} = \left[-sfp'\left(\frac{1}{B} - \frac{B}{\langle B^2\rangle}\right)\right]B + \frac{B^2}{\langle B^2\rangle}\langle \vec{j}\cdot\vec{B}\rangle \tag{1.13}$$

The term in brackets in equation (1.13) is the Pfirsh-Schluter current, j_{PS}, representing the parallel current required to return the poloidal current needed to balance the pressure gradient.

$$\vec{j}\cdot\vec{B} = j_{PS}B + \frac{B^2}{\langle B^2\rangle}\langle \vec{j}\cdot\vec{B}\rangle \tag{1.14}$$

Both the terms on the right hand side of (1.13) result in an order ϵ=a/R variation in $\vec{j}\cdot\vec{B}$ relative to its flux surface average.

2. 'Kinetic' MHD Equilibrium Solution

Taking the flux surface average of Ampère's law, equations (1.7), gives an expression for the flux surface average toroidal current density in terms of the parallel current minus a poloidal current contribution (which, as was discussed above, is small)

$$j_{TOR} \equiv \langle\frac{j_\varphi R_0}{R}\rangle = \frac{\langle\vec{j}\cdot\vec{B}\rangle}{f/R_0} - \left(-s\,\langle\frac{{B_p}^2}{\mu_0}\rangle\,\frac{f'}{f/R_0}\right) \equiv j_{PAR} - j_{POL} \tag{2.1}$$

where R_0 is a characteristic major radius. For DIII-D, R_0 is taken as the center of the vacuum vessel = 1.6955m. From the force balance and equations (1.9) and (1.10), j_{TOR} and j_{PAR} can be expressed as

$$j_{TOR} \equiv \langle\frac{j_\varphi R_0}{R}\rangle = -s\left[R_0 p' + \frac{ff'}{\mu_0 R_0}\langle\frac{R_0^2}{R^2}\rangle\right] \tag{2.2a}$$

$$j_{PAR} \equiv \frac{\langle\vec{j}\cdot\vec{B}\rangle}{f/R_0} = -s\left[R_0 p' + \frac{ff'}{\mu_0 R_0}\frac{\langle B^2\rangle}{(f/R_0)^2}\right] \tag{2.2b}$$

$$j_{POL} = j_{PAR} - j_{TOR} = -s\left[\frac{ff'}{\mu_0 R_0}\frac{\langle {B_p}^2\rangle}{(f/R_0)^2}\right] \tag{2.2c}$$

Using

$$\langle\frac{{B_p}^2}{\mu_0}\rangle = \frac{sI(\psi)}{V_P} \tag{2.3}$$

where $I(\psi)$ is the signed toroidal current within a given flux surface, the current densities can be written in terms of the enclosed currents

$$j_{TOR} = \frac{R_0}{V_P}I'(\psi), \qquad j_{PAR} = \frac{R_0}{V_P}f\left(\frac{I}{f}\right)', \qquad j_{POL} = -\frac{R_0}{V_P}\frac{f'}{f}I(\psi)\,, \tag{2.4}$$

$$I(\psi) = \frac{1}{R_0}\int_{\psi_0}^{\psi} V_P\, j_{TOR}\,d\,\psi' = \frac{f}{R_0}\int_{\psi_0}^{\psi}\frac{V_P}{f}\, j_{PAR}\,d\,\psi' \tag{2.5}$$

Given that j_{TOR} can be computed a priori, the usual technique for constructing a kinetic equilibrium is to use it only to set the current density in the edge H-mode pedestal region, with the current density in the core and the plasma shape being determined from MSE plus external magnetic measurements in a 'free-boundary' equilibrium fit (EFIT fitting mode). Generally MSE and external magnetics alone do not allow the pedestal current density profile to be determined accurately enough for edge stability studies. EFIT allows the average current density

$$j_{EFIT} \equiv \bar{j_\varphi} = \frac{I'}{A'} = \langle\frac{j_\varphi R_0}{R}\rangle / \langle\frac{R_0}{R}\rangle = j_{TOR}/\langle\frac{R_0}{R}\rangle \tag{2.6}$$

to be set as a constraint on the equilibrium at a number ψ locations. Typically about 10 current constraint points are placed in the H-mode pedestal region for a kinetic fit.

Alternately the flux surface average of the force balance, equation (1.9), can be used to solve for ff' over the entire plasma cross-section

$$\frac{ff'}{\mu_0 R_0} = \left(-s\,\langle\frac{j_\varphi R_0}{R}\rangle - R_0 p'\right) / \langle\frac{R_0^2}{R^2}\rangle \tag{2.7}$$

with the plasma boundary shape specified (EFIT equilibrium mode where p' and ff' are fully specified in terms of spline functions). This approach has the disadvantage that the core current density profile cannot be determined accurately since it is subject to long current diffusion times and the effects of MHD modes. Even when one is only interested in edge stability, inaccuracy in the central current density profile can significantly affect the pedestal region though such things as its effect on the mapping between flux space and physical space where the pressure profile measurements are made.

As will be seen in the next section j_{PAR} can be computed from Ohm's law plus expressions for the bootstrap and neutral beam and RF driven currents but this computation, as well as j_{POL}, is dependent on the MHD equilibrium. An iterative scheme is therefore used where j_{PAR} and j_{POL} are computed from the previous iteration's equilibrium,

$$j_{TOR}|_n = j_{PAR}(n, T, ..; \psi|_{n-1}) - j_{POL}|_{n-1} \tag{2.8}$$

where the 0th equilibrium is a magnetics only EFIT. In practices the differences between a magnetics only and kinetic fit only weakly affect j_{PAR} while j_{POL} is a small so that the equilibrium iterations converge rapidly. In fact it is often only necessary to compute j_{TOR} from j_{PAR} and j_{POL} using a magnetics only EFIT.

3. Computing j_{PAR}

The generalized expression for Ohm's law for a single ion species neglecting viscosity and electron inertia from Braginskii[2] is

$$\vec{E} + \vec{V} \times \vec{B} = \frac{\vec{J_\parallel}}{\sigma_\parallel} + \frac{\vec{J_\perp}}{\sigma_\perp} + \frac{1}{n_e e}\left[\vec{j} \times \vec{B} - \left(\nabla p_e - \overrightarrow{R_T}\right)\right] \tag{3.1}$$

Taking the parallel component of (3.1) and adding the non-inductive currents gives

$$\vec{j} \cdot \vec{B} = \sigma_\parallel^{NEO} \vec{E} \cdot \vec{B} + \vec{j}_{BS} \cdot \vec{B} \;\; + \vec{j}_{CD} \cdot \vec{B} \tag{3.2}$$

where $\sigma_\parallel^{NEO}$ is the neoclassical parallel conductivity (see section 5), $\vec{j}_{BS}$ is the bootstrap current, and $\vec{j}_{CD}$ is the current driven by neutral beams and RF. Taking the flux surface average gives

$$j_{PAR} = \sigma_\parallel^{NEO} \frac{\langle \vec{E} \cdot \vec{B} \rangle}{f/R_0} + \frac{\langle \vec{j}_{BS} \cdot \vec{B} \rangle}{f/R_0} + \frac{\langle \vec{j}_{CD} \cdot \vec{B} \rangle}{f/R_0} \equiv j_{OH} + j_{BS} + j_{CD} \tag{3.3}$$

Following the notation of the ONETWO transport code[7]

$$E_0 \equiv \frac{\langle \vec{E} \cdot \vec{B} \rangle}{f/R_0 \langle R_0^2/R^2 \rangle}, \qquad \sigma_0 \equiv \sigma_\parallel^{NEO} \langle R_0^2/R^2 \rangle \tag{3.4}$$

giving

$$j_{PAR} = \sigma_0 E_0 + j_{BS} + j_{CD} \tag{3.5}$$

As previously mentioned, the core current density profile is assumed to be well determined from an equilibrium using only MSE plus external magnetics, and the kinetic analysis seeks to set the current density in the pedestal region. So j_{PAR} need only be computed in the pedestal region, defined as being between the flux ψ_M and the separatrix at ψ_S, with boundary conditions given by the toroidal current enclosed within these two surfaces. The current drive contribution in the H-mode pedestal region is generally quite small and therefore a time independent value from an average over the ELM cycle can be used or it can be neglected entirely. j_{CD} is retained in the analysis to allow smaller values of ψ_M to be used under some conditions.

The general solution for E_0 is difficult since, even for a fixed plasma boundary shape and fixed toroidal field, there are affects from current diffusion, the change in the shape of the internal flux surfaces due to changes in the current distribution, and changes in the toroidal flux distribution due to changes in plasma β. A precise determination of E_0 would involve a full calculation of the current profile evolution: solving Faraday's law from the beginning of the discharge while maintaining the discharge in MHD equilibrium at every time step. Although this is possible with the ONETWO transport code it is not a tractable approach for studying the H-mode pedestal stability in at a large number of discharge conditions.

An approximate approach is taken in solving for j_{OH} and E_0. We limit ourselves to discharges that are steady state except perhaps for an ELM cycle affecting the pedestal region. We also assume that the ELM effects are relatively small; having negligible impact on the overall plasma β or the total plasma current in the core region. Based on these assumptions we take the poloidal flux surfaces to be fixed in shape and the toroidal flux to be constant in time throughout the plasma. These assumptions implies from Faraday's law that

$$-\left.\frac{d\phi}{dt}\right|_{\psi} = \oint E_{POL} dl = V_p \langle E_{POL} B_{POL} \rangle = 0 \tag{3.6}$$

giving

$$E_0 \equiv \frac{\langle E_\varphi B_\varphi \rangle}{f/R_0 \langle R_0^2/R^2 \rangle} = \frac{\langle R E_\varphi R_0^2/R^2 \rangle / R_0}{\langle R_0^2/R^2 \rangle} \tag{3.7}$$

With the shape of the flux surfaces fixed in time, the loop voltage

$$V_L = 2\pi R E_\varphi \tag{3.8}$$

is a flux function, so that

$$E_0 = V_L(\psi)/2\pi R_0 \tag{3.9}$$

Giving

$$j_{PAR} = \sigma_0 V_L / 2\pi R_0 + j_{BS} + j_{CD} \tag{3.10}$$

A further simplification is to take V_L to be spatially constant in the pedestal region. Although this would seem to be questionable due to the variation in the bootstrap current, $j_{BS} \propto \nabla p$, during the ELM cycle and resulting back EMF, time dependent analysis has shown that, at moderate heating power, the Ohmic current density in the pedestal is fully relaxed by the time of the next ELM. Although increasing the plasma density increases the ELM frequency, this also decreases the pedestal temperature shortening the current diffusion time. V_L=constant is more questionable at high heating power or if one is interested in the period shortly after an ELM. V_L as a spatial constant can be either input to the code, perhaps from the experimentally measured value, or determined from the total plasma current as described below. An example of the components of j_{TOR} is shown in Fig. 1a.

Using equation (2.5) the total plasma current is given by

$$I_P = I(\psi_M) + \frac{f_S V_L}{2\pi R_0^2}\int_{\psi_M}^{\psi_S} \frac{V_P}{f}\sigma_0 d\,\psi' + \frac{f_S}{R_0}\int_{\psi_M}^{\psi_S} \frac{V_P}{f}(j_{BS} + j_{CD}) d\,\psi' \tag{3.11}$$

where $f_S = f(\psi_S)$, which can be solved for V_L

$$V_L = \frac{I_P - I_M - I_{BS} - I_{CD}}{\frac{f_S}{2\pi R_0^2}\int_{\psi_M}^{\psi_S} \frac{V_P}{f}\sigma_0 d\,\psi'} \tag{3.12}$$

In the case where relaxation of the Ohmic current in the pedestal during the ELM cycle is important we start with the form of Faraday's law derived for the ONETWO transport code[7]

$$\frac{\partial B_{P0}}{\partial t} = \frac{\partial E_0}{\partial \rho} \tag{3.13}$$

where

$$\phi = \frac{f_S}{R_0}\pi\rho^2 = B_{T0}\pi\rho^2, \;\; B_{P0} = \frac{1}{R_0}\frac{\partial \psi}{\partial \rho} \tag{3.14}$$

Solving equation (3.5) for E_0 and expressing j_{PAR} in terms of the enclosed toroidal current using equation (2.4)

$$\frac{\partial B_{P0}}{\partial t} = \frac{\partial}{\partial \rho}\left(\frac{1}{\sigma_0}\left[2\pi R_0 f \frac{1}{V'}\left(\frac{I}{f}\right)' - j_{BS} - j_{CD}\right]\right) \tag{3.15}$$

The enclosed current can be expressed in terms of B_{P0}

$$I = \frac{2\pi}{\mu_0}\rho H G B_{P0}\,, \qquad \frac{\partial V}{\partial \rho} = 4\pi^2 R_0 \rho H, \qquad G = \frac{\langle {B_p}^2 \rangle}{{B_{P0}}^2}, \qquad H = \frac{F}{\langle R_0^2/R^2 \rangle}\,, \qquad F = f_S/f \tag{3.16}$$

Substituting (3.16) into (3.15) gives the relaxation equation for B_{P0} to be solved on the region between ψ_M and ψ_S with boundary condition determined by the enclosed current relation (3.16) (note that $B_{P0} = 0$ at the separatrix but GB_{P0} remains finite and obeys (3.16))

$$\frac{\partial B_{P0}}{\partial t} = \frac{\partial}{\partial \rho}\left(\frac{1}{\sigma_0}\left[\frac{1}{\mu_0}\frac{f}{H\rho}\frac{\partial}{\partial \rho}\left(\frac{H\rho}{f}GB_{P0}\right) - j_{BS} - j_{CD}\right]\right) \tag{3.17}$$

The equilibrium is not evolved as the pedestal current responds to the changes in profile during the ELM cycle with G, H, f and j_{CD} taken to be independent of time; however σ_0 and j_{BS} vary with the temperature and density profiles. The solution of (3.17) is not yet implemented in efit_kinetic.py but requires a time dependent run of the ONETWO transport code. The module onetwo.py handles combining a time series of profile fits through the ELM cycle into a series of ELM periods (typically 5 ELM periods are used to allow the initial magnetics only current profile in the pedestal to damp away) and running ONETWO which directly provides j_{TOR} (see section 8).

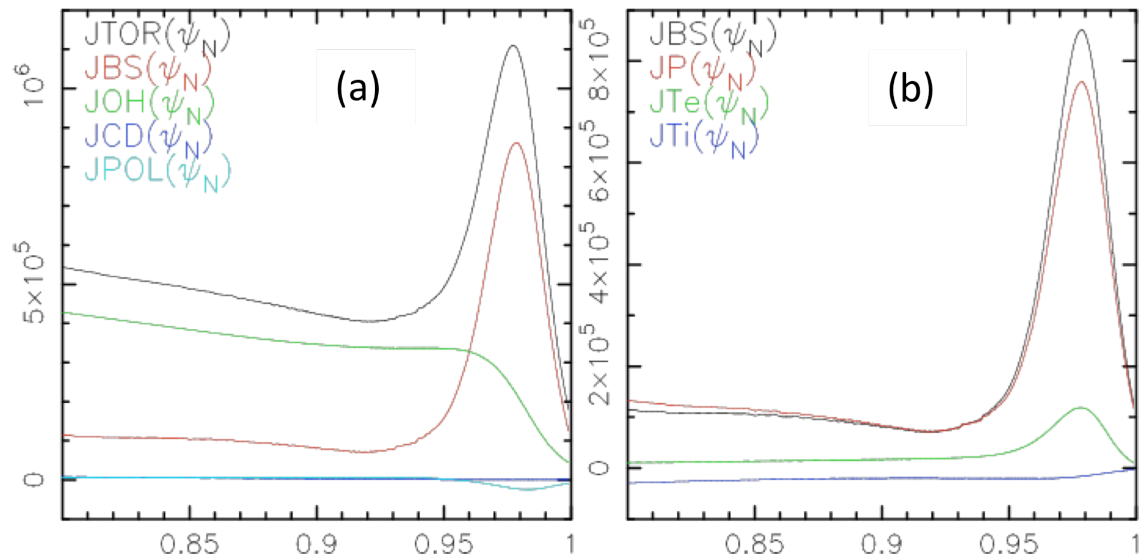

FIG. 1 (a) Components of JTOR as described in section 3 including the bootstrap, JBS, Ohmic, JOH, current drive, JCD, and poloidal current, JPOL, current density contributions versus normalized poloidal flux. (b) Pressure gradient, JP, Te gradient, JTe, and Ti gradient, JTi contributions to the bootstrap current density, JBS as described in section 4.

A rough estimate of the pedestal current relaxation time is given by

$$\tau \sim \mu_0 \sigma_0 \Delta_\rho^2 \sim 6 T_e^{\frac{3}{2}} \Delta_\rho^2 \left(\frac{ms}{keV\, cm^2}\right) \tag{3.18}$$

where Δ_ρ is the pedestal width in ρ space. For DIII-D Δ_ρ ~ 1-3cm and $T_e \lesssim 1$ keV so τ ~ 10s of ms which is often short compared to the length of the inter-ELM period.

4. Expressions for j_{BS}

j_{BS} is computed in the module efit_jsauter.py using both the Sauter[3] model and a recent refinement of Sauter based on runs of the XGC0 drift kinetic particle code by Koh, et. al[4]. The Koh model includes a more detailed treatment of the pedestal region where the ion banana width is on the order of the gradient scale length and is more accurate in the region very close to the separatrix where effects of the electron banana width come into play. The Koh model departs from Sauter as the pedestal collisionality is increased. At higher collisionality on DIII-D the Koh mode predicts a reduction in j_{BS} relative to Sauter, while at the low aspect ratio of NSTX a larger and opposite trend is predicted. In actual discharges even on NSTX however, the difference between the Sauter and Koh models does not generally have a large impact on the net pedestal current since the bootstrap current is reduced roughly as $1/\nu_{*e}$ and so the net pedestal current density becomes dominantly Ohmic.

The expressions for j_{BS} can be broken into terms which depend on the density gradient plus temperature gradient terms, or equivalently into a pressure gradient term plus temperature gradient terms. The later arrangement is taken in efit_jsauter.py as pressure gradient term is generally strongly dominant; an example is show in Fig. 1b.

$$j_{BS} = j_P + j_{Te} + j_{Ti} = -R_0 p_e (g_P + g_{Te} + g_{Ti}) \tag{4.1}$$

Where the g terms are related to the gradient scale lengths

$$g_P = L_{31}\frac{1}{p_e}\frac{\partial p}{\partial\psi}, \quad g_{Te} = L_{32}\frac{1}{T_e}\frac{\partial T_e}{\partial\psi}, \quad g_{Ti} = L_{34}\alpha\frac{1-p_e/p}{p_e/p}\frac{1}{T_i}\frac{\partial T_i}{\partial\psi} \tag{4.2}$$

and p is the thermal pressure, i.e. excluding fast ions. The coefficients $L_{31}, L_{32}, L_{34}, \alpha$ are functions of the electron and ion collisionalities, ν_{*e} ,ν_{*i}, and the trapped particle fraction, f_t. With $\epsilon(\psi) = \frac{a}{R}$ and n_e in units of $10^{20}/m^3$and T_e in units of keV unless otherwise noted

$$\nu_{*e} = 6.921 \times 10^{-4}\frac{qRn_eZ\Lambda_e}{\epsilon^{1.5}T_e^2}, \quad \Lambda_e = 15.18 - \ln\left(\frac{n_e^{1/2}}{T_e}\right) \tag{4.3}$$

$$\nu_{*i} = 4.900 \times 10^{-4}\frac{qRn_i\widetilde{Z}_i^{\,4}\Lambda_i}{\epsilon^{1.5}T_i^2}, \quad \Lambda_i = 17.34 - \ln\left(\frac{\widetilde{Z}_i^{\,3}n_i^{1/2}}{T_i^{3/2}}\right) \tag{4.4}$$

where

$$n_i = \sum n_k, \qquad \bar{Z} = \frac{n_e}{n_i}, \qquad Z \equiv Z_{eff} = \sum Z_k^2\frac{n_k}{n_e}, \qquad \widetilde{Z}_i = \left(Z_i^2\bar{Z}Z\right)^{1/4} \tag{4.5}$$

and Z_k, n_k are the charge and density of the kth ion species, while Z_i is the main ion charge. Although both the Sauter[3] and Koh[4] models deal with only a single ion species, the effects of collisions between multiple ion species are included in the terms n_i and $\widetilde{Z}_i$, as described in Koh[4], based on comparisons to the NCLASS model.

The effective trapped particle fraction is given by [4]

$$f_t = 1 - \frac{3}{4}\int_0^1 \frac{\lambda d\lambda}{\langle(1-\lambda h)^{\frac{1}{2}}\rangle} \tag{4.6}$$

where $h = \frac{B}{B_{MAX}}$ is the ratio of the magnetic field to its maximum value on a given flux surface. Equation (4.6) is difficult to evaluate numerically due to the double integral, however an accurate estimate of (4.6) was developed[5] from upper and lower bounds

$$f_t = 0.75 f_{tu} + 0.25 f_{tl} \tag{4.7a}$$

$$f_{tu} = 1 - \langle h^2\rangle\langle h\rangle^{-2}\left[1-(1-\langle h\rangle)^{\frac{1}{2}}(1+0.5\langle h\rangle)\right] \tag{4.7b}$$

$$f_{tl} = 1 - \langle h^2\rangle\langle h^{-2}\left[1-(1-h)^{1/2}(1+0.5h)\right]\rangle \tag{4.7c}$$

In the Koh model f_t is adjusted near the separatrix to take into account the effect of electron banana orbit width,

$$f_t^{XGC} = f_t H(\psi) \tag{4.8a}$$

$$H_{Toward} = 1 - \frac{0.2}{Z^4}\exp\left(-\left|\frac{1-\hat{\psi}}{W_{be}}\frac{1}{2.7\ln(\epsilon^{1.5}\nu_{*e}/3.2+3)}\right|\right) \tag{4.8b}$$

$$H_{Away} = 1 - \frac{0.6}{Z^4}\exp\left(-\left|\frac{1-\hat{\psi}}{W_{be}}\frac{1}{3.3\ln(\epsilon^{1.5}\nu_{*e}+2)}\right|\right) \tag{4.8c}$$

Where (4.8b) is appropriate for ∇B drift toward the X-point and (4.8c) is for drift away from the X-point, $\hat{\psi}$ is the normalized poloidal flux (0 at magnetic axis and 1 at separatrix) and

$$W_{be} = \frac{\partial\hat{\psi}}{\partial R}\frac{\epsilon^{0.5}v_{th,e}}{\frac{e|B_P|}{m_e}} = \left(\frac{2m_e\epsilon T_e(eV)}{e}\right)^{\frac{1}{2}}\frac{R}{\psi_{sep}-\psi_{axis}} \tag{4.9}$$

is the electron banana width in terms of normalized poloidal flux. $W_{be}\sim 10^{-4}$, while the other terms in the exponential are ~ 1/3 so H only has an effect very near the separatrix and is negligible near the pedestal current density peak. Returning to the coefficients in equation (4.2) and letting

$$z_1 = \frac{1}{Z+1} \tag{4.10}$$

gives from reference [3]

$$L_{31} = \left(\left((0.2z_1 f_{31} + 0.3z_1)f_{31} - 1.9z_1\right)f_{31} + 1.4z_1 + 1\right)f_{31} \tag{4.11}$$

$$f_{31} = \frac{f_t}{1+(1-0.1f_t)\nu_{*e}^{1/2} + 0.5(1-f_t)\nu_{*e}/Z} \tag{4.12}$$

$$L_{34} = \left(\left((0.2z_1 f_{34} + 0.3z_1)f_{34} - 1.9z_1\right)f_{34} + 1.4z_1 + 1\right)f_{34} \tag{4.13}$$

$$f_{34} = \frac{f_t}{1+(1-0.1f_t)\nu_{*e}^{1/2} + 0.5(1-0.5f_t)\nu_{*e}/Z} \tag{4.14}$$

$$L_{32} = F_{32\_ee} + F_{32\_ei} \tag{4.15}$$

$$F_{32\_ee} = \frac{0.05+0.62Z}{Z(1+0.44Z)}\left(f_{32\_ee} - f_{32\_ee}^4\right) + \frac{1.2}{1+0.5Z}f_{32\_ee}^4$$

$$+\frac{1}{1+0.22Z}\left[f_{32\_ee}^2 - f_{32\_ee}^4 - 1.2\left(f_{32\_ee}^3 - f_{32\_ee}^4\right)\right] \quad (4.16)$$

$$f_{32\_ee} = \frac{f_t}{1+0.26(1-f_t)\nu_{*e}^{1/2} + 0.18(1-0.37f_t)\nu_{*e}/Z^{0.5}} \quad (4.17)$$

$$F_{32\_ei} = \frac{-(0.56+1.93Z)}{Z(1+0.44Z)}\left(f_{32\_ei} - f_{32\_ei}^4\right) - \frac{1.2}{1+0.5Z} f_{32\_ei}^4$$

$$+\frac{4.95}{1+2.48Z}\left[f_{32\_ei}^2 - f_{32\_ei}^4 - 0.55\left(f_{32\_ei}^3 - f_{32\_ei}^4\right)\right] \quad (4.18)$$

$$f_{32\_ei} = \frac{f_t}{1+(1+0.6f_t)\nu_{*e}^{1/2} + 0.85(1-0.37f_t)\nu_{*e}(1+Z)} \quad (4.19)$$

In the Koh model[4]

$$f_{31}^{XGC} = f_{31}(1+\delta), \quad f_{34}^{XGC} = f_{34}(1+\delta), \quad f_{32\_ee}^{XGC} = f_{32\_ee}(1+\delta), \quad f_{34\_ei}^{XGC} = f_{34\_ei}(1+\delta) \quad (4.20)$$

where

$$\delta = 0.55Z^{0.2}(1-e^{-10\nu_{*e}})\tanh\left(\frac{3.2\beta\epsilon^{2.1}\nu_{*e}^{1.4}}{Z^{\xi}}\right)\tanh\left(\frac{2.2\beta\epsilon^{2.8}\nu_{*e}^{0.1}}{Z^{\xi}}\right) \quad (4.21a)$$

$$\beta = Re[(\epsilon - 0.44)^{0.7}] \quad (4.21b)$$

$$\xi = \frac{-Z^2+5.998Z-4.981}{4.298Z^2-14.07Z+12.61} : Z \le 5, \qquad \xi = 0 : Z > 5 \quad (4.21c)$$

The final coefficient for the ion temperature gradient term of equation (4.2) is given in [3] as

$$\alpha = \frac{\dfrac{\alpha_0 + 0.25\nu_{*i}^{1/2}(1-f_t^2)}{1+0.5\nu_{*i}^{1/2}} + 0.315\nu_{*i}^2 f_t^6}{1+0.15\nu_{*i}^2 f_t^6}, \qquad \alpha_0 = \frac{-1.17(1-f_t)}{1-0.22f_t-0.19f_t^2} \quad (4.22)$$

The Koh model corrections to Sauter are only important at higher collisionality as shown by a plot of δ from equation (4.21) in Fig 2. We also see from this figure that the corrections minimize at about Z=2 and increase for both higher and lower Z. There is also a strong effect of aspect ratio where for DIII-D the corrections are rather small and tend to reduce the bootstrap current, while for NSTX they can be large and tend to increase the bootstrap current.

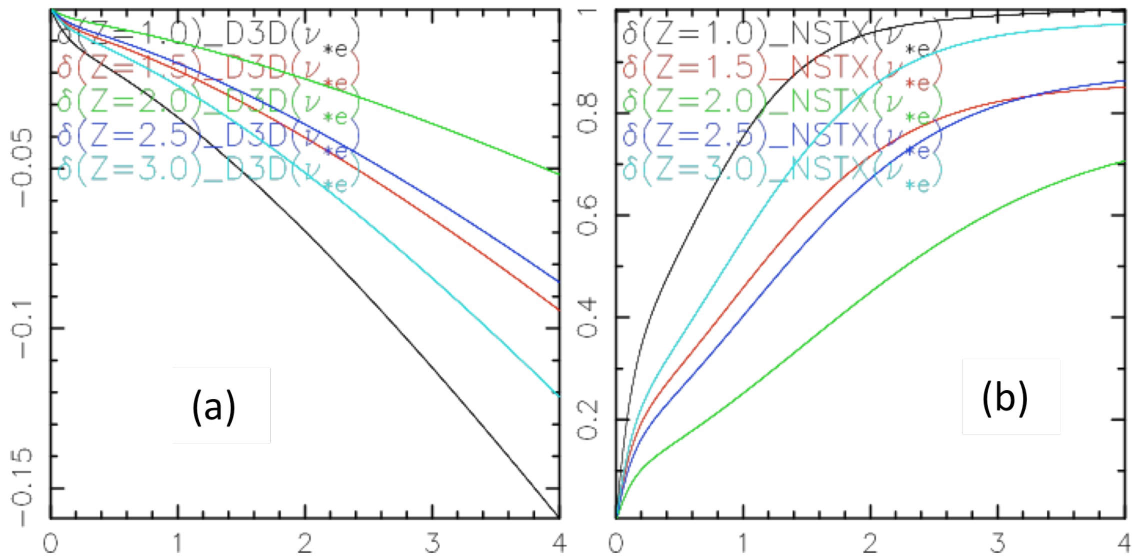

FIG. 2 Dependence of Koh model[4] correction term δ given in equation (4.21) as a function of electron collisionality for several Z values at (a) DIII-D and (b) NSTX aspect ratios.

5. Expression for conductivity σ_0

σ_0 can be computed from equation (3.4) given an initial equilibrium and an expression for the neoclassical parallel conductivity which can be found in Sauter[3]

$$\sigma_{\parallel}^{NEO} = F_{33}\sigma_{\parallel}^{Spitzer} \tag{5.1}$$

where

$$\sigma_{\parallel}^{Spitzer} = 6.012 \times 10^{8} \frac{T_e^{3/2}}{ZN\Lambda_e} \tag{5.2}$$

$$N = \frac{0.74}{Z + 0.76} + 0.58 \tag{5.3}$$

and

$$F_{33} = 1 + \left((-0.23 f_{33}/Z + 0.59/Z) f_{33} - 0.36/Z - 1\right) f_{33} \tag{5.4}$$

$$f_{33} = \frac{f_t}{1 + (0.55 - 0.1 f_t)\nu_{*e}^{1/2} + 0.45(1 - f_t)\nu_{*e}/Z^{1.5}} \tag{5.5}$$

6. Important quantities for edge stability

Safety factor:

$$q = \frac{1}{2\pi}\frac{d\phi}{d\psi} = \frac{\rho B_{t0}}{R_0 B_{p0}} = \frac{fV'}{4\pi^2}\langle\frac{1}{R^2}\rangle = \frac{f_s V'}{4\pi^2 H R_0^2} \tag{6.1}$$

Normalized pressure gradient:

$$\alpha = \frac{B_{t0}^2 \rho_V V'}{4\pi^2}\frac{\partial\beta}{\partial\psi} = H R_0 q^2 \frac{\rho_V}{\rho}\frac{\partial\beta}{\partial\rho}, \qquad \beta = \frac{p}{B_{t0}^2/2\mu_0} \quad , \quad \rho_V \equiv \sqrt{\frac{V}{2\pi^2 R_0}} \tag{6.2}$$

For DIII-D ρ_V/ρ is roughly a constant independent of ρ.

Magnetic shear:

$$S = 2\frac{V}{V'}\frac{q'}{q} = \frac{V}{2\pi^2 R_0 \rho H}\frac{1}{q}\frac{\partial q}{\partial\rho} = \frac{2V}{2\pi^2 R_0 \rho^2 H}\left[1 - \left(\frac{\rho}{2B_{p0}}\right)\frac{1}{\rho}\frac{\partial(\rho B_{p0})}{\partial\rho}\right] \tag{6.3}$$

Defining a current density and average current density in analogy to the cylindrical case

$$j_0 \equiv \frac{1}{\mu_0\rho}\frac{\partial(\rho B_{p0})}{\partial\rho}, \qquad \bar{j_0} \equiv \frac{\int 2\pi\rho j_0 d\rho}{\pi\rho^2} = \frac{2B_{p0}}{\mu_0\rho} \tag{6.4}$$

$$S = \frac{2V}{2\pi^2 R_0 \rho^2 H}\left[1 - \frac{j_0}{\bar{j_0}}\right] \tag{6.5}$$

So the shear is controlled by the relationship between the local and average current density, crossing 0 when these are equal. The relation of j_0 to the previously defined currents is complex however since

$$j_{TOR} = \frac{1}{\mu_0\rho H}\frac{\partial(\rho H G B_{p0})}{\partial\rho}, \qquad j_{PAR} = \frac{f}{\mu_0\rho H}\frac{\partial(\rho H G B_{p0}/f)}{\partial\rho} \tag{6.6}$$

The form for the flux surface average current density which is important for peeling-ballooning stability includes a contribution from the Pfirsh-Schluter current; from equation (1.14)

$$j_{ELITE} \equiv \frac{f}{R_0}\langle\frac{\vec{j}\cdot\vec{B}}{B^2}\rangle = \frac{f}{R_0}\langle\frac{j_{PS}}{B}\rangle + \frac{\left(\frac{f}{R_0}\right)^2}{\langle B^2\rangle} j_{PAR} = -s\left[R_0 p'\left(\frac{f}{R_0}\right)^2\langle\frac{1}{B^2}\rangle + \frac{ff'}{\mu_0 R_0}\right] \tag{6.7}$$

In the usual ELITE plots the current in 6.7 is normalized to the average current density $j_{AV} = I(\psi)/A(\psi)$ and the mean of this normalized current at the pedestal current peak and separatrix is used.

$$j_{ELITE}^N \equiv \frac{j_{ELITE}|_{Max-Ped} + j_{ELITE}|_{Sep}}{2j_{AV}} \tag{6.8}$$

This term should affect shear in an analogy to equation (6.5).

The second stable regime for infinite-n ideal ballooning modes is reached roughly when the shear normalized to q^2 is below a critical value

$$s = \frac{S}{q^2} \lesssim 0.15 \tag{6.9}$$

7. efit_jsauter.py module inputs and outputs

The python module efit_jsauter.py is used to compute j_{TOR} from both the Sauter[3] and Koh[4] models for j_{BS}. It is called automatically in the kinetic EFIT module efit_kinetic.py. efit_jsauter.py takes as inputs a set of profiles, and EFIT geqdsk data. The geqdsk data is from the previous kinetic EFIT iteration as discussed in relation to equation (2.8). The profile set and geqdsk data can be obtained in the proper structure using the modules best_profiles.py and efit_eqdsk.py. An example is shown below.

```
>>> import efit_jsauter,efit_eqdsk,best_profiles
>>> p = best_profiles.get_best_profs(153152,2450,'e8099')
>>> g = efit_eqdsk.get_gdat(153152,2480,efit='KINETIC')
>>> j = efit_jsauter.jsauter(p,g,psijfix=0.8)
efit_jsauter.jsauter: Using jXGC0 form with Grad-B drift toward the X-point.
efit_jsauter.jsauter: Using j profile from input geqdsk inside psin = 0.80.
efit_jsauter.jsauter: Determining vloop, joh by matching total Ip.
efit_jsauter: Ip(MA)=1.38, Ifix=1.11, Ibs     =0.11, Ioh     =0.16, Idrive=0.00, E0     =3.86e-02, Vl     =0.411
efit_jsauter: Ip(MA)=1.38, Ifix=1.11, Ibs_xgc=0.10, Ioh_xgc=0.17, Idrive=0.00, E0_xgc=3.90e-02, Vl_xgc=0.420
```

Here the profiles set, p, and the geqdsk data, g, are read from MDSplus but reading from a pfile and geqdsk file is also possible. best_profiles.get_best_prof also allows manipulation of the profiles, for example scaling the pedestal pressure up and down at constant collisionality, which is useful for edge stability studies

The returned python dictionary, j, is keyed with strings and has values which are Data class instances representing profiles as a function of normalized poloidal flux, ψ_N, as for example shown in Fig. 1. A complete list of the output profiles is given below.

1/B**2	<1/B^2>
B**2	<B^2>
F32_ee	Term in L32, equation (4.16), Sauter model.
F32_ei	Term in L32, equation (4.18), Sauter model.
F32_xgc_ee	Term in L32, equation (4.16), Koh model.
F32_xgc_ei	Term in L32, equation (4.18), Koh model.
F33	Coefficient in sneo, equation (5.4)
L31	Coefficient to gp, equation (4.11), Sauter model.
L31_xgc	Coefficient to gp, equation (4.11), Koh model.
L32	Coefficient to gte, equation (4.15), Sauter model.
L32_xgc	Coefficient to gte, equation (4.15), Koh model.
L34	Coefficient to gti, equation (4.13), Sauter model.
L34_xgc	Coefficient to gti, equation (4.13), Koh model.
R	Major radius
Rpe	pe/pth used in coefficient to gti, equation (4.2).
a	Minor radius
alf	Coefficient in gti, equation (4.2,4.22).
alf0	Term in alf, equation (4.22).
ap	d(Cross-sectional-Area)/dpsi

beta_xgc	Term in Koh correction to ft, equation (4.21b)
dIbs	d(Ibs)/dpsi, Ibs=enclosed bootstrap current, Sauter model.
dIbs_xgc	d(Ibs)/dpsi, Ibs=enclosed bootstrap current, Koh model.
dIdrive	d(Idrive)/dpsi, Idrive=enclosed driven current.
dIoh	d(Ioh)/dpsi, Ioh=enclodse Ohmic current.
delta_xgc	Term in Koh correction to ft, equation (4.211)
dpth	d(pth)/dpsi
dte	d(Te)/dpsi
dti	d(Ti)/dpsi
f31	Term in L31, equation (4.12), Sauter model.
f31_xgc	Term in L31, equation (4.12), Koh model.
f32_ee	Term in F32_ee, equation (4.17), Sauter model.
f32_ei	Term in F32_ei, equation (4.19), Sauter model.
f32_xgc_ee	Term in F32_ee, equation (4.17), Koh model.
f32_xgc_ei	Term in F32_ei, equation (4.19), Koh model.
f33	Term in F33, equation (5.5).
f34	Term in L34, equation (4.14), Sauter model.
f34_xgc	Term in L34, equation (4.14), Koh model.
ffprim	ff'
fpol	Bt*R
ft	Trapped particle fraction, equation (4.7).
ft0	(a/R)^0.5
ft_xgc	ft modified by Koh factor = ft*h_xgc, equation (4.8).
ftl	Lower bound term in ft, equation (4.7c)
ftu	Upper bound term in ft, equation (4.7b)
fz	n_Carbon/n_e
gp	Pressure gradient term, equation (4.2), Sauter model.
gp_xgc	Pressure gradient term, equation (4.2), Koh model.
gte	Te gradient term, equation (4.2), Sauter model.
gte_xgc	Te gradient term, equation (4.2), Koh model.
gti	Ti gradient term, equation (4.2), Sauter model.
gti_xgc	Ti gradient term, equation (4.2), Koh model.
h	<B/Bmax> used in ft calculation, equation (4.7).
h2	<B^2/Bmax^2> used in ft calculation, equation (4.7).
h_xgc	Koh model modification factor for ft, equation (4.8).
hf	Second term in <> equation (4.7c), used in ft calculation
ip	Total current within a flux surface.
j12	JTOR, equation (2.1), Sauter model, = CURDEN from ONETWO
j12_xgc	JTOR, equation (2.1), Koh model.
jb	CURDRIVE from ONETWO, jdrive = jb*FCAP
jbs	JBS, equation (4.1), Sauter model. = CURBOOT*FCAP from ONETWO
jbs_xgc	JBS, equation (4.1), Koh model.
jdrive	JCD, equation (3.3), = CURDRIVE*FCAP from ONETWO.
jef	JEFIT, average j used in EFIT, equation (2.5), Sauter model.
jef_xgc	JEFIT, average j used in EFIT, equation (2.5), Koh model.
joh	JOH, Ohmic current, quation (3.3), Sauter model.
joh_xgc	JOH, Ohmic current, quation (3.3), Koh model.
jp	Pressure gradient contribution to JBS, equation (4.1), Sauter model.
jp_xgc	Pressure gradient contribution to JBS, equation (4.1), Koh model.
jpol	JPOL, equation (2.1).

jst	JPAR, equation (2.1,3.3), Sauter model, = CURPAR*FCAP from NETWO
jst_xgc	JPAR, equation (2.1,3.3), JOH model.
jte	Te gradient contribution to JBS, equation (4.1), Sauter model.
jte_xgc	Te gradient contribution to JBS, equation (4.1), Koh model.
jti	Ti gradient contribution to JBS, equation (4.1), Sauter model.
jti_xgc	Ti gradient contribution to JBS, equation (4.1), Koh model.
lambdae	Electron log(lambda), equation (4.3).
lambdai	Ion log(lambda), equation (4.4).
ne	Electron density.
ni	n_D + n_C used in ion collisionality, equation (4.5)
nustare	Electron collisionality, equation (4.3).
nustari	Ion collisionality, equation (4.4).
pb	Fast ion pressure.
pe	Electron pressure.
pth	Thermal pressure.
ptot	Total pressure = pth + pb.
q	Safety factor
rm1	<1/R>
rm2	<1/R^2>
rp2	<R^2>
sneo	Neoclassical parallel conductivity, equation (5.1).
sspitz	Spitzer parallel conductivity, equation (5.2).
te	Electron temperature.
ti	Ion temperature.
vl	Loop voltage, equation (3.12), Sauter model.
vl_xgc	Loop voltage, equation (3.12), Koh model.
vp	dV/dpsi/(2pi), equation (1.11)
wbe_xgc	Electron banana width width, equation (4.9), Koh model.
zeff	Z effective, equation (4.5).

The returned Data class objects have many useful attributes and methods. See the data.py module for documentation. For example they can be dumped to an ASCII file with

```
>>> j[ ‘jef’ ].dump()
```

Or plotted using the screens module

```
>>> import screens
>>> s = Screen( __name__ , j )
>>> s.ad(  j[ ‘jef’ ] )
>>> s.pl()
```

8. ONETWO code related parameters

Current densities computed in the ONETWO transport code can be related to the quantities used in this memo. The geometric quantities $FCAP,$ $GCAP,$ and $HCAP$ are given by the expressions F, G, H in equation (3.16). The current densities are related as

$$j_{TOR} = CURDEN \times FCAP \quad (8.1)$$

$$j_{PAR} = CURPAR \times FCAP \quad (8.2)$$

$$j_{BS} = CURBOOT \times FCAP \quad (8.3)$$

$$j_{CD} = CURDRIVE \times FCAP \quad (8.4)$$

The Ohmic component in ONETWO is defined such that toroidal current is the sum of the Ohmic, bootstrap, and current drive rather than the parallel current as given by equation (3.3) and so mixes in a contribution from the poloidal current density

$$CURDEN = CUROHM + CURBOOT + CURDRIVE \quad (8.5)$$

$$j_{OH} = FCAP\ (CURPAR - CURBOOT - CURDRIVE) \quad (8.6)$$

$$j_{POL} = FCAP\ (CURPAR - CURDEN) = \ j_{OH} - \ CUROHM \times FCAP \quad (8.7)$$

9. Running efit.py to produce a kinetic EFIT

Running efit.py to produce an MHD equilibrium using EFIT with the pressure profile from measurements and edge current density constrained by the bootstrap current models as described above is discussed in detail here: https://diii-d.gat.com/diii-d/PyD3D/apps/efit#Kinetic_EFITs. The method is briefly described below.

efit.py creates a keqdsk input file for EFIT containing the pressure profile from profile analysis of the experimental data and with j_{EFIT}, as defined in equation (2.5) and determined as described in the sections above, specified at a number of points in the H-mode pedestal region. The keqdsk input file also contains the external magnetics and MSE data which has been averaged in time over the same intervals used for the pressure profile construction. The pressure is input at 132 points with packing into the steep gradient region of the pedestal as a function of normalized poloidal flux in the variables RPRESS and PRESSR in the IN1 namelist. $j_{EFIT}/(\frac{I_P}{Area})$ is specified at about 10 locations in the pedestal region, with location set in the variable SIZEROJ and value in VZEROJ in the INWANT namelist in the keqdsk file. The location of the current constraint points are generally set automatically by the code but sometimes adjustment of the innermost points is needed for EFIT convergence. EFIT is run in fitting mode with p’ and ff’ represented by splines. Up to 16 spline knots can be used but generally the default of 9 knots is sufficient. The location of the knots is normally automatically set by efit_kinetic.py with the exception of the innermost knot which often needs to be adjusted to achieve good EFIT convergence. As j_{EFIT} and the mapping between the profile measurement locations and poloidal flux space depends implicitly on the equilibrium, the process is iterated adjusting the profiles and other terms to changes in the flux geometry in the kinetic fit. An example solution is shown in figure 3.

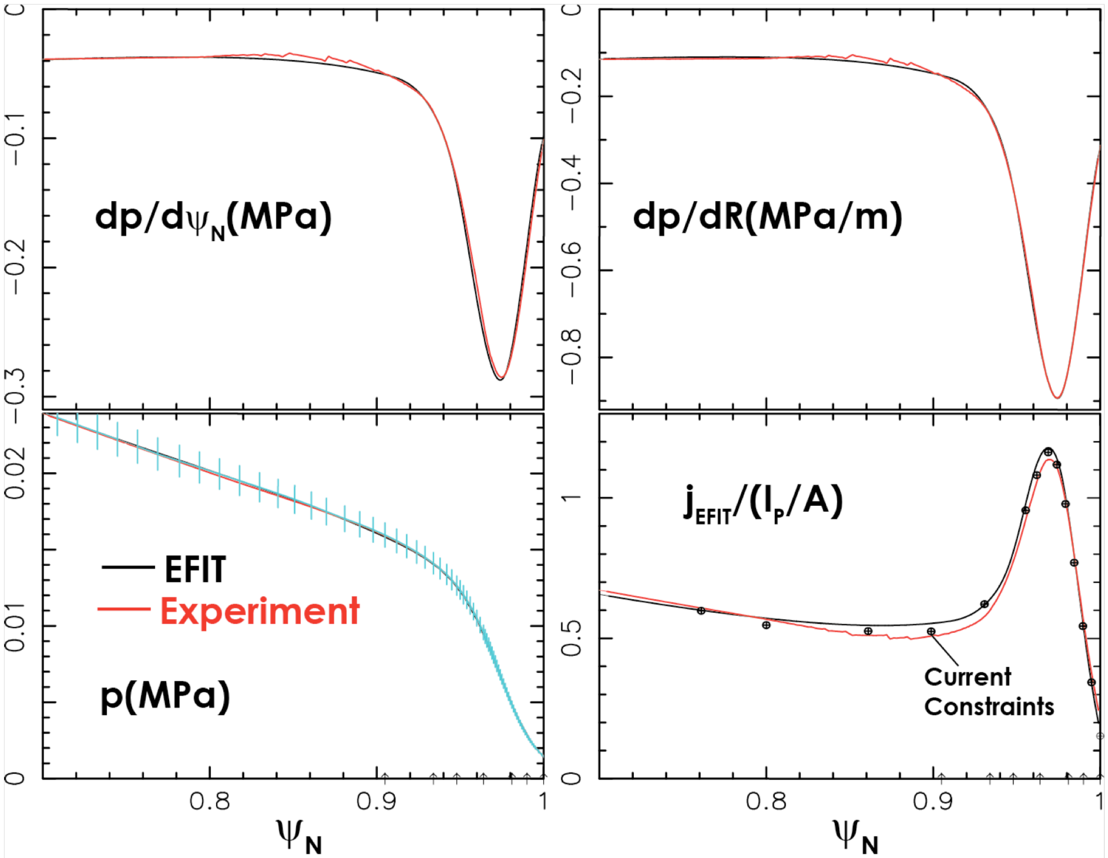

Fig. 3 Match between 'experimental' profiles shown as red curves and EFIT equilibrium shown as black curves. a) Total pressure profile; experimental profile mapping is adjusted in the iteration process described in the text. Error bars show relative weighting and point packing of input pressure profile points to EFIT. b) $dp/d\psi_N$, a match between experiment and EFIT indicates spline functions well represents the input pressure profile, c) dp/dR, a match indicates good agreement between actual profile in physical space and kinetic EFIT, d) normalized current density profile showing the location of the constraints.

REFERENCES

[1] D.M. Thomas, Rev. Sci. Inst., **74**, 1541 (2002).

[2] S.I. Braginskii, Rev. Plasma Phys., **V1**, Consultants Bureau, 267 (1965).

[3] O. Sauter, C. Angioni, and Y.R. Lin-Liu, Phys. Plasmas, **6**, 2834 (1999).
ERRATA: O. Sauter, C. Angioni and Y.R. Lin-Liu, Phys. Plasmas, **9**, 5140 (2002).

[4] S. Koh, C.S. Chang, et. al, Phys. Plasmas, **19**, 072505-1 (2012).

[5]S.P. Hirshman and D.J. Sigmar, Nucl. Fusion **21**, 1079 (1981).

[6] Y.R. Lin-Liu and R.L. Miller, Phys. Plasmas, **2**, 1666 (1995).

[7] W.W. Pfeiffer, R.H. Davidson, R.L. Miller, and R.E. Waltz, "ONETWO: A Computer Code for Modeling Plasma Transport in Tokamaks", **GA-A16178** (1980).

[8] L.L. Lao, et al., Nucl. Fusion **30**, 1035 (1990).